Chinese Journal of Chemical Engineering 32 (2021) 212–223

Contents lists available at ScienceDirect

Chinese Journal of Chemical Engineering

journal homepage: www.elsevier.com/locate/CJChE

Article

2-Hydroxy-1, 4-napthoquinone solubilization, thermodynamics and adsorption kinetics with surfactant

Zoya Zaheer *, Ekram Yousif Danish, Samia A. Kosa

Department of Chemistry, Faculty of Science, P. O. Box 80203, King Abdulaziz University, Jeddah 21589, Saudi Arabia

ARTICLE INFO

Article history:
Received 3 March 2020
Received in revised form 12 August 2020
Accepted 7 September 2020
Available online 23 November 2020

Keywords:
Adsorption
Aggregation
Lawsone
Surfactant
Solubilization
Kinetics

ABSTRACT

2-Hydroxy-1, 4-napthoquinone (lawsone) natural red–orange dye was extracted from fresh henna (Lawsonia inermis) leaves in an alkaline media. The lawsone-surfactant solubilization constants (K_{LS}) were calculated for the first time by using cationic cetyltrimethylammonium bromide (CTAB) and anionic sodium dodecyl sulphate (SDS). The standard free energy, concentration of solubilized lawsone and number of lawsone molecules solubilized into micelles were calculated and discussed. Surface excess, minimum surface area per molecule, surface pressure, free energy (adsorption and aggregation) and equilibrium constants of different states were determined from tensiometry. Different metal ions (Ag^{+}, Co^{2+}, Cu^{2+}, Ni^{2+}, Fe^{3+}, Zn^{2+} and Al^{3+}) were used to determine the complex forming ability with lawsone. Out of these, Ag^{+} ions have strong binding capacity with lawsone. The adsorption of lawsone on the surface of glass with silver ions in presence of CTAB was also observed at pH $\geq$ 9.0. The pseudo-first, second-order kinetic equation, intraparticles diffusion and Elovich models were used to determine the kinetics of lawsone adsorption onto the surface of glass and a probable mechanism has been discussed. Lawsone adsorption followed second-order kinetic equation (k_2 = 0.019 g·mg^{-1}·min^{-1}).

1. Introduction

Henna (Lawsonia inermis) is an ancient dye and used for the coloration of skin, hair, eyebrows and other body human part on festivals and marriages occasions. The henna name was derived from the Arabic word *hinna*. It is commonly called as *Mehndi, Chinah, Mandee, Al-khanna, tien kao, mohuz* etc. all over the different region. The green leaves past has been used to prevent various infections such as ulcers, constipating, leucoderma, anemia, small pox, leprosy and skin inflammation from ancient time [1]. Lawsone (2-Hydroxy-1, 4-napthoquinone; red–orange dye; natural orange 6; slightly water soluble; simple molecule with non-ionic groups) is a main active chemical constituent of henna leaves that has an affinity towards protein binding, leading to a strong stain at ambient conditions and also used for dyeing in textile industries [2]. Hydroxynapthoquinone and its derivatives have strong coordination ability towards metal ions and acted as a redox active ligands [3]. The metal complexation of lawsone required alkaline media and coordination ability depends on the nature of base [4,5]. Hijji *et al.* reported that the various (CN^{-}, CH_3COO^{-}, F^{-}, $H_2PO_4^{-}$ and HSO_4^{-}) changed the color of aqueous lawsone solution in water-acetonitrile (95:5), whereas Cl^{-}, Br^{-}, I^{-} and ClO_4^{-} has no significant effect and suggested that the CN^{-} and CH_3COO^{-} formed excellent sensor [6]. Kumar and his-coworkers used lawsone to the synthesis of azo dye and prepared a colorimetric sensor for the detection of copper(II) and iron(III) ions by using fluorescence spectroscope [7]. Jelly *et al.* developed a lawsone based reagent for the detection of latent fingerprints on the surface of paper [8]. Lawsone reacts with protein and developed color, which exhibiting photolemenisence activities [9].

The coloration of substrates has been the principle application of dyes in textile industries. For dyeing processes, the presence of a suitable organized aggregates (micelles, vesicles and layers) are essential for the solubilzation of hydrophilic and hydrophobic dyes [10–18]. For example, Simoncic and Kert reported the interaction of acid orange 7 and acid red 88 with cationic and non-ionic surfactants and suggested that the surfactant formed a complex with ionic dyes as well as felicitate the adsorption of nonionic dyes [13]. Das and his coworkers extracted the natural dyes from mangifera indica, glochidion lanceolarium and litsea sebifera plants and reported the dye interaction with cationic and anionic surfactants [17]. Mohammad *et al.* used Lawsonia inermis leaves and Rubia cordifolia roots for the extraction of natural dyes and

* Corresponding author.
E-mail address: zzkhan@kau.edu.sa (Z. Zaheer).

https://doi.org/10.1016/j.cjche.2020.09.064

suggested that the henna extract shows excellent antifungal activities on the wool substrate [18]. Aksu *et al.* used dried Rhizopus arrhizus to the removal of methylene blue by adding sodium dodecyl sulphate and suggested that the Freundlich adsorption isotherm exhibited better dye uptake than the Langmuir isotherm [19].

Sangeetha and Philip was used lawsone as a capping agent for the preparation of Fe_3O_4 nanoparticles in presence of cysteine as a linker. The Fe_3O_4-cysteine-lawsone nanocomplex exhibited excellent corrosion as well as antimicrobial activity [20]. Lawsone sensitized solar cell were fabricated by using, TiO_2, Zn and AgNPs [21–23]. Incorporation of NPs in the solar cell enhanced electron life time. Barani *et al.* was prepared lawsone based noisome and used as a nano-herbal drug for the treatment of breast cancer [24]. The complex formation between dye and metal ions provide significant information related to the fastness of color in dyeing textile industries [25]. The removals of toxic and non-biodegradable dyes by using a large number of adsorbents have been reported on several occasions for different point of view [26–30]. Ghaedi *et al.* used adsorption phenomenon for the removal of congo red in presence of carbon supported nanoadsorbent of silver, palladium and zinc [31]. Recently, we extracted juglone [32] and betanin [33] from the walnut shell powder and beetroots, respectively, and used for the fabrication of silver nanoparticles and removal of congo red. Silver and iron were prepared for the adsorption and degradation of acid orange 7 and bromothymol blue dyes [34,35]. However, no information was available in the literature regarding the adsorption of lawsone from an aqueous solution. Despite the excellent applications of lawsone in sensing, forensic science, coordination, medicinal, textile, and pharmaceutical industries, the interaction of lawsone with ionic surfactants has been neglected.

In the present study, Henna leaves were used for the extraction of red–orange lawsone dye. The interactions of lawsone with cationic and anionic surfactants have been investigated. For this purpose, CTAB and SDS were chosen as model surfactants and various parameters were determined and discussed. To determine the mechanism of lawsone sorption on the surface of glass, various kinetic models (pseudo-first order, pseudo-second order, intraparticle diffusion Weber and Morris model and Elovich equation were used. Incidentally, this study became the first report for the lawsone-surfactant interactions and its adsorption on the surface of glass with silver(I) in presence of cationic CTAB surfactant. The adsorption of dye provides valuable information about the improvement of color strength and colour fastness properties of lawsone in presence of a suitable surface active agent.

2. Experimental and Procedure

2.1. Chemicals

Cetyltrimethylammonium bromide (CTAB), sodium dodecyl sulphate (SDS) sodium hydroxide (NaOH, for pH adjustment), sulphuric acid (H_2SO_4), silver nitrate ($AgNO_3$, oxidizing agent), lawsone ($C_{10}H_6O_3$, reducing agent), inorganic electrolytes (NaCl, NaBr, $NaNO_3$, NaI) and complex forming metal ions (Cu^{2+}, Zn^{2+}, Ni^{2+}, Co^{2+}, Fe^{3+} and Al^{3+}) analytical grade were received from Sigma-Aldrich and BDH and used without further purification. The aqueous solutions of all reagents were prepared on the molarity basis and double distilled water was used as solvent.

2.2. Extraction of lawsone

In the perspective of existed literature, better shading yield in the event of soluble extraction of lawsone, yellow–red dye was extracted from henna leaves in an alkaline condition maintained by adding required amount of sodium carbonate. Henna fresh leaves were collected from the garden of the university and authenticated by the department of biological sciences. To remove the dust particles, ten grams leaves were washed under tap water followed by distilled water, dried under room temperature. The powder of henna leaves were taken in a round bottom flask containing an 100 ml aqueous solution of Na_2CO_3 (for maintaining pH ca. 8.0 to 9.0) and heated at 80 °C for 30 min with occasional stirring. The green suspension of henna leaves and water turned brown. The suspension was left over night and filtered by using a clean cotton cloth. The remaining residue was again treated with Na_2CO_3 aqueous solution, heated and filtered for several time. The resulting brown color was again extracted by using diethyl ether and dried with magnesium sulphate. For the solid lawsone, the ether was removed from rotatory evaporator and reddish material was obtained. The stock solution of lawsone was prepared in water and a calibration plot was constructed for the calculation of molar extinction coefficient.

2.3. Instruments

Shimadzu UV-260 spectrophotometer was used to record the UV–visible spectra of lawsone under various experimental conditions. Fourier Transform infrared spectrophotometer (Burker Tensor) was used to determine the functional groups of extracted lawsone in the range 4000–400 cm^{-1}. KBr disk was prepared with few drops of lawsone solution and dried at room temperature before the measurements. The resulting spectra were compared with the authentic samples of lawsone purchased from Sigma-Aldrich. The 400 MHz Brucker spectrometer was used for the measurement of ^1H nuclear magnetic resonance (NMR) spectra of lawsone. Fisher Scientific Accumet Digital pH meter (model 910) was used for pH measurements. The platinum ring detachment method was used to measure the surface tension of different solutions (CTAB, CTAB + lawsone, SDS, and SDS + lawsone) on Kruss 11Tensiometer. The instrument was calibrated with double distilled water (surface tension = 73.2 $mN\cdot m^{-1}$ at 25 °C) [36]. Electrical conductivities of CTAB in pure water and in lawsone aqueous solution were determined by assembly of conductivity meter (AC-13 Japan) with a conductivity cell (cell constant = 0.943 cm^{-1}). The conductivity meter was calibrated by using 0.01 $mol\cdot L^{-1}$ aqueous solution of KCl at 25 °C prior to use.

2.4. Solubilization of lawsone into surfactants

Lawsone is a natural dye with benzenoid and quinonide rings, soluble in water (1.15×10^{-2} $mol\cdot L^{-1}$ [6]) and solubility increases with pH. To see insight into the incorporation of lawsone into the various aggregates of CTAB and SDS, the UV–visible spectra of henna extract was recorded with increasing concentration of surfactant. The critical micellar concentration of CTAB and SDS was calculated from the intersection of the two straight lines. Various parameters such as dye-surfactant binding constant, solubilization rate constant, amount of solubilized dye into the micelles and number of dye molecules incorporated in a single micelle were estimated with standard models.

2.5. Batch adsorption studies

In order to see insight the color change and/or color fastness of lawsone aqueous solution, NaOH solution was added into the dye. The absorbance of working solution was increased dramatically and the resulting red–orange was stable for ca. one month. In the next experiment, CTAB solution (5.0 ml of 0.01 $mol\cdot L^{-1}$; total volume 40 ml) was added in a conical flask containing dye (4.0×10^{-4}

mol·L^{-1}) and NaOH (2.0 ml of 0.01 mol·L^{-1}). The UV–visible spectrum of each solution was measured as a function of time. Thirdly, the same experiment was repeated with silver nitrate (5.0 ml of 0.01 mol·L^{-1}). Surprisingly, dye adsorption began to starts as the reaction time increases and a thick red layer of dye adsorbed on glass surface of the conical flask. The dye adsorption was estimated quantitatively with reported method [31]. The same experiment was repeated with different metal ions (Cu^{2+}, Zn^{2+}, Ni^{2+}, Co^{2+}, Fe^{3+} and Al^{3+}) individually. We did not observe the deposition of red layer on the glass surface

3. Results and Discussion

3.1. UV–visible data

The color intensity, number of absorption peaks and position of wavelength maxima (λ_{max}) of lawsone red–orange pigment depends on the nature of the organic solvents as well as pH of the aqueous solution. UV–visible spectra of extracted lawsone were recorded in under different conditions to establish the role of cationic and anionic surfactants. Fig. 1A shows that the lawsone spectrum exhibits one sharp absorption peak at 268 nm along with two week shoulder at ca. 330 and 450 nm in water. A red shift was observed from 268 to 300 nm (total 32 nm) with increasing the

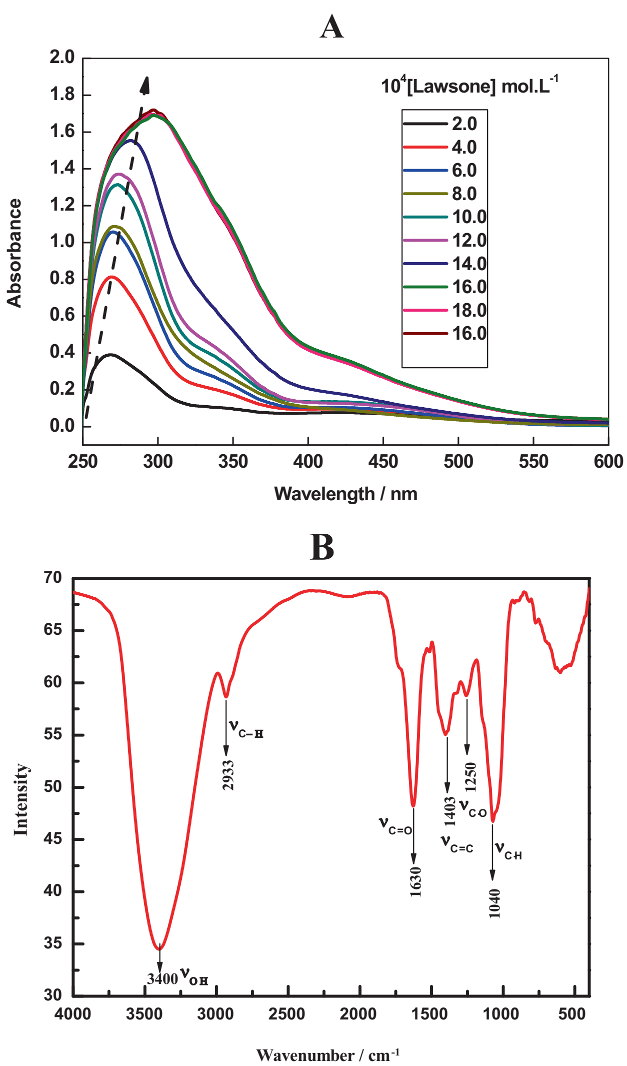

Fig. 1. UV–visible spectra of lawsone in water at 30 °C (A) and its FTIR spectrum (B).

[lawsone], indicating the aggregation and association of lawsone molecules. A calibration plot was constructed to determine the molar extinction coefficient of lawsone by using Beer-Lambert law. The plot between absorbance and [lawsone] is liner at lower concentration ($\leq 8.0 \times 10^{-4}$ mol·L^{-1}) but it deviates from the linearity as the [lawsone] increases from 8.0×10^{-4} to 10.0×10^{-4} mol·L^{-1} (positive chemical deviation), which might be due to the existence of different absorbing species of lawsone in equilibrium. The molar extinction coefficient (ε = 1539 mol^{-1}· dm^3· cm^{-1}) was calculated from the initial linear part of Fig. S1 (Supplementary Material). The FTIR spectrum of extracted lawsone is now given in Fig. 1B. The main peaks are observed at 3400, 2933, 1630, 1403, 1250 and 1040 cm^{-1} are assigned to ν_{OH}, $\nu_{C\text{-}H}$, $\nu_{C=O}$, $\nu_{C=C}$, $\nu_{C\text{-}O}$ and $\nu_{C\text{-}H}$ respectively, for symmetric and asymmetric vibrations [3]. The ^{1}H NMR spectra of lawsone was recorded by using 400 MHz Brucker spectrometer in dimethyl sulfoxide (DMSO-d_6) at room temperature. Lawsone ^{1}H NMR showed the singlet at 6.16 δ for H-3 and multiple doublet and triplet for 4H of benzene ring (Fig. 2) [37].

UV–visible spectra of lawsone were measured as different pH (ranging from 6.6 to 12.2) adjusted by adding H_2SO_4 and NaOH. It was observed that the absorbance was increases with increasing the pH of the working solution (Fig. 3A). As the pH of the reaction mixture increases, the absorbance at 280 nm increases with red shift (from 276 to 308 nm) and a new peak began to develop at ca. 450 nm. Interestingly, the absorbance of peak at 450 nm was also increases with pH (Fig. 3B), which can be rationalized due to the higher solubility of lawsone in alkaline media [38]. At lower pH ($\leq$4.0), the lawsone aqueous solution is colourless. It shows a pale yellow color at neutral pH. Hijji and his coworkers reported that the UV–visible spectra of lawsone shows only one peak at 333 nm in acetonitrile, whereas one absorption peak and strong shoulder was appeared at 333 and 450 nm in acetonitrile–water (95/5) mixture [6].

The pale yellow color also became orange. The intensity of color increases with pH and aqueous solution became dark orange, and the resulting color was stable for ca. two months. On the basis of above results, the following ionization of lawsone was proposed (Fig. 4).

Fig. 4 shows the ionization of lawsone in an aqueous solution. At lower pH ($\leq$4.0), lawsone solution is colorless. As the pH increases, the ionization of C2-OH takes place, which leads to the formation of anionic form of lawsone. Due to the presence of conjugated system between the C2, C3 and C4, the anionic species (1, 4-naphthoquinone; less stable due to the repulsion between the partial negative charge of C1 carbonyl oxygen and the negative charge of C2 enolic oxygen) was stabilized via resonance and equilibrium shift in favor of more stable 1, 2-napthoquinone formation. As a result, lawsone exhibited red–orange color in an alkaline media.

In order to establish the lawsone-surfactant interaction and/or solubilisation, a series of UV–visible spectra of CTAB + lawsone

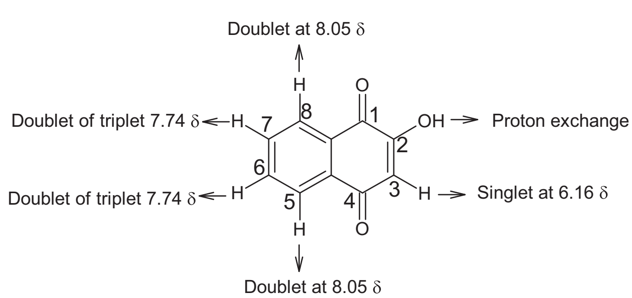

Fig. 2. Structure of lawsone.

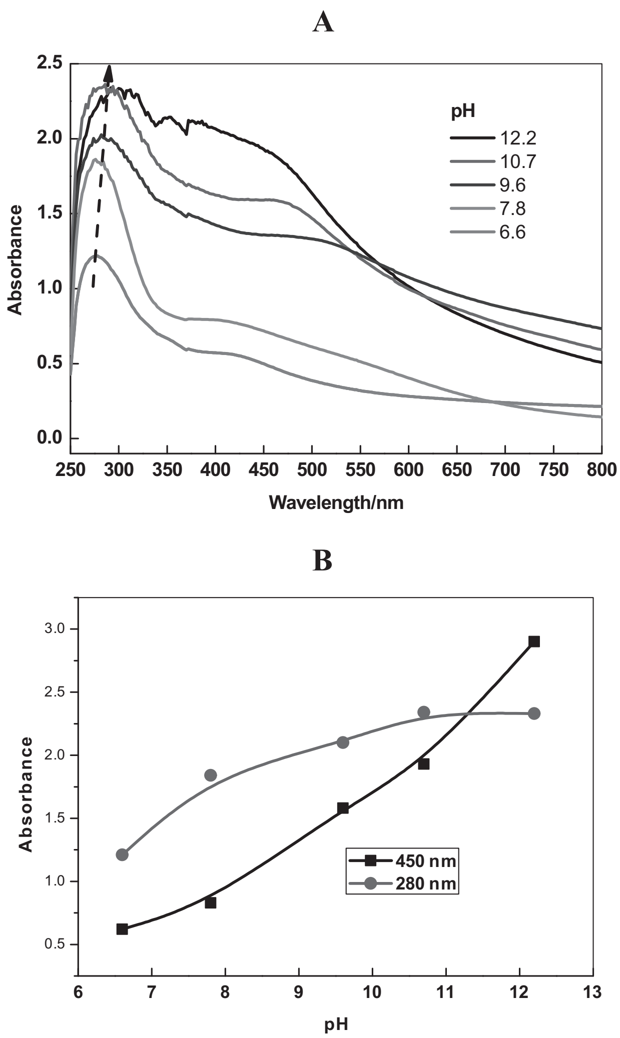

Fig. 3. UV–visible spectra of lawsone as a function of pH (A) and absorbance-pH profiles of lawsone aqueous solution (B). Reaction conditions: [lawsone] = 4.0 × 10^{-4} mol· L^{-1}.

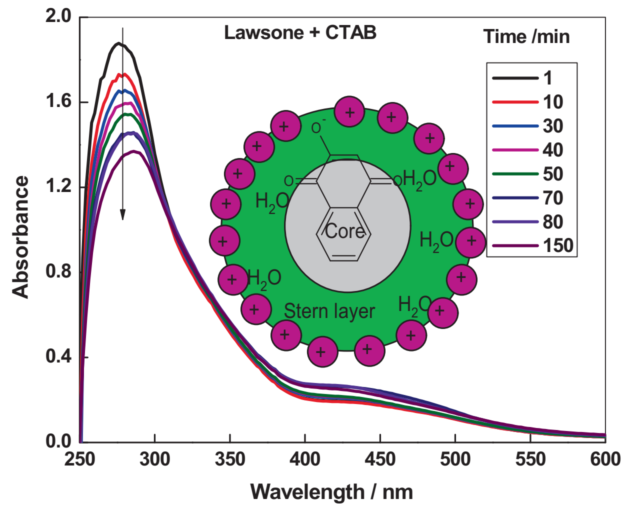

Fig. 5. UV–visible spectra of lawsone in presence of CTAB as a function of time at 30 °C. Reaction conditions: [CTAB] = 12.5 × 10^{-4} mol·L^{-1} and [lawsone] = 4.0 × 10^{-4} mol. L^{-1}.

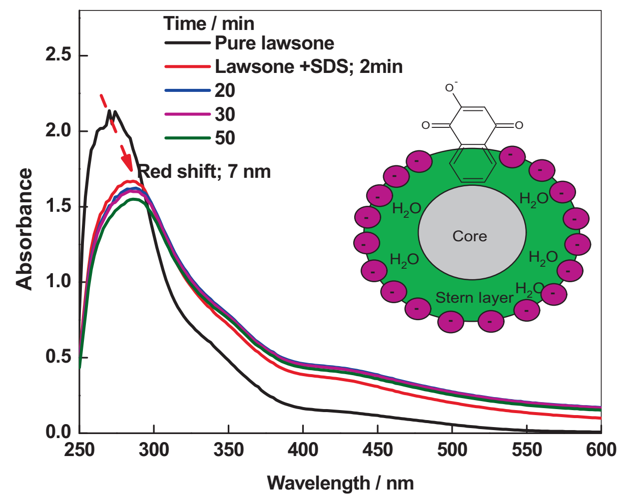

Fig. 6. UV–visible spectra of lawsone in presence of SDS as a function of time at 30 °C. Reaction conditions: [SDS] = 12.5 × 10^{-4} mol· L^{-1} and [lawsone] = 4.0 × 10^{-4} mol·L^{-1}.

and SDS + lawsone were recorded for different [surfactant] as a function of time. Surprisingly, the peak intensity decreases with time after the addition of both surfactants in an aqueous solution of dye (Figs. 5 and 6). The decrease of the absorbance (hypochromic shift) can be rationalized to the complex formation between lawsone and surfactant [39]. For CTAB, the λ_{max} position of dye did not change but peak intensity decreases with time (Fig. 5). On the other hand, a red shift (total 7 nm) was observed with SDS (Fig. 6). The different behaviour might be due to the significant role of polar head groups of surfactant in the solubilisation of dye. Interestingly, the decay in the peak absorbance with time indicates that the complexation and/or solubilisation are slow processes.

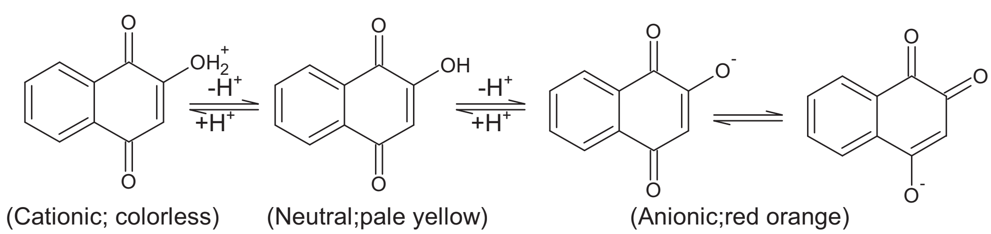

Fig. 4. Ionization of lawsone in an aqueous solution.

The Benisi-Hildebrand model was used to determine the binding constant (K_S), which was described in the literature (Eqs.1 and 2) [40].

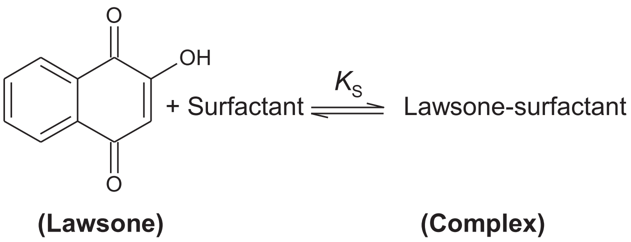

(1)

where surfactant = $CH_3(CH_2)_{15}N(CH_3)_3Br$(CTAB) and $CH_3(CH_2)_{10}$-CH_2OSO_3Na (SDS) Eq. (2) can be derived from Eq. (1).

$$K_S = [\text{Complex}]/[\text{Lawsone}][\text{surfactant}] \quad (2)$$

Benisi-Hildebrand derived the following relation for the evaluation of K_S.

$$\frac{1}{(A_{obs} - A_0)} = \frac{1}{(A_c - A_0)} + \frac{1}{K_S(A_c - A_0)[\text{surfactant}]} \quad (3)$$

where all symbols have their usual significance. Thus, the double reciprocal plot between $1/(A_{obs} - A_0)$ and 1/[surfactant] should be linear with a slope equal to $1/K_S\ (A_c{-}A_0)$ and an intercept equal to $1/(A_c{-}A_0)$. The values of K_S were calculated from the slopes and intercepts of Fig. 7A and B, respectively, for CTAB and SDS and found to be 1.1×10^3 and 1.8×10^2 $L{\cdot}mol^{-1}$. CTAB has ten times higher solubilizing capacity than that of SDS. It was observed that the plots of $1/(A_{obs} - A_0)$ and 1/[surfactant] were linear at higher concentrations ($\geq$0.0003 $mmol{\cdot}L^{-1}$ and 0.003 $mmol{\cdot}L^{-1}$) for CTAB and SDS. At lower concentrations, no linearity was observed.

To calculate the K_S and $\Delta\varepsilon$ (difference between the molar absorption coefficient between the free and solubilized lawsone), Connett and Wetterhahn model was also used [41]. They proposed Eq. (4) for the evaluation of associated parameters.

$$\frac{[\text{Lawsone}][\text{surfactant}]}{\Delta(\text{Absorbance})} = \frac{[\text{surfactant}]}{\Delta\varepsilon l} + \frac{1}{K_S\Delta\varepsilon l} \quad (4)$$

where Δ(Absorbance) = difference between the absorbance of unsolubilized and solubilized lawsone at the same λ_{max} and l = path length (1.0 cm). The $\Delta\varepsilon$ and K_S values were estimated from the slopes and intercepts of [lawsone] [surfactant]/ Δ(Absorbance) versus [surfactant] (Fig. 8A and B). These are given in Table 1.

Further, the K_S values were also calculated with Bouguera-Lamberta-Beera rule (Eq. (5)) [39,42].

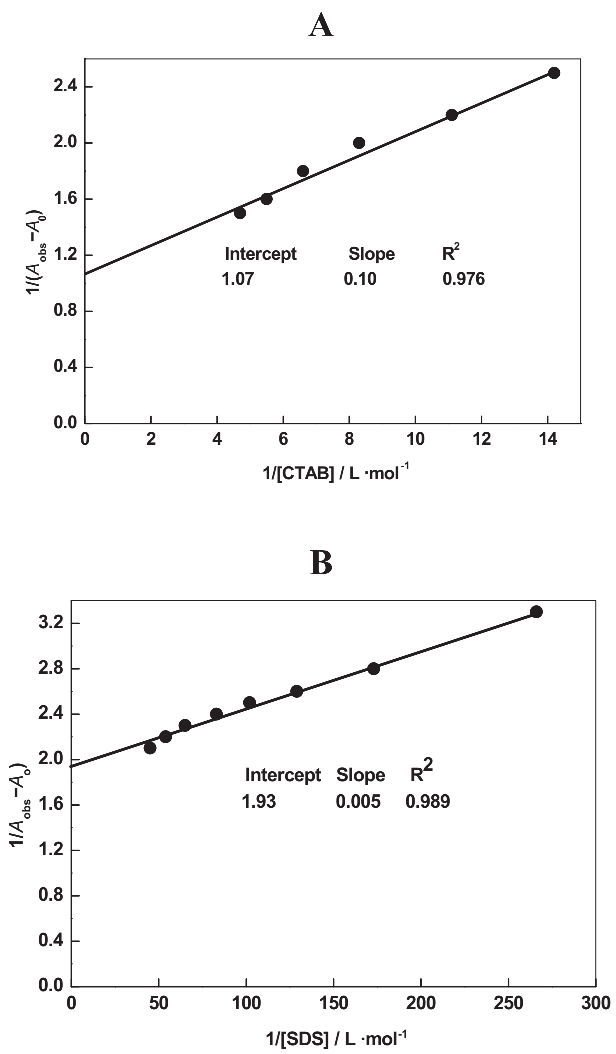

Fig. 7. Benesi-Hildebrand plot to the solubilization of lawsone into CTAB (A) and SDS (B). Reaction conditions: [lawsone] = 4.0×10^{-4} $mmol{\cdot}L^{-1}$.

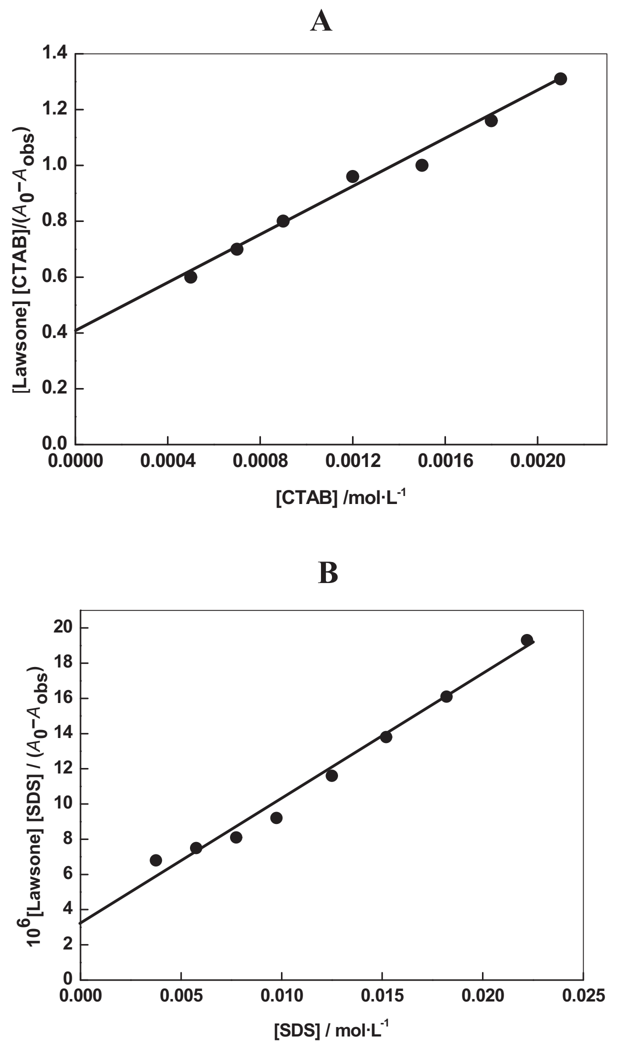

Fig. 8. Connett-Wetterhahn plot to the solubilization of lawsone into CTAB(A) and SDS (B). Reaction conditions: [lawsone] = 4.0×10^{-4} $mmol{\cdot}L^{-1}$.

Table 1
Values of surfactant-lawsone solubilization parameters calculated by UV–visible spectroscopic data 30 °C

Parameters	CTAB	SDS
CMC/mmol·L^{-1}	8.1×10^{-4}	7.9×10^{-3}
K_S/L· mol^{-1}; Benisi-Hildebrand	1.1×10^{3}	3.8×10^{2}
K_S/L·mol^{-1}; Connett-Wetterhahn	1.1×10^{3}	1.8×10^{2}
K_S/L·mol^{-1}; Bouguera-Lamberta-Beera	1.2×10^{3}	7.4×10^{2}
$\Delta\varepsilon$/mmol·L^{-1}·cm^{-1}	2275	1394
D_m/mol·L^{-1}	2.2×10^{-4}	3.1×10^{-4}
m/mol·L^{-1}	5.0×10^{-6}	7.1×10^{-5}
n	44	4
ΔG^0/kJ·mol^{-1}	−17.6	−15.0
ΔG^0/kJ·mol^{-1}	−17.6	−13.0
ΔG^0/kJ·mol^{-1}	−17.8	−16.6

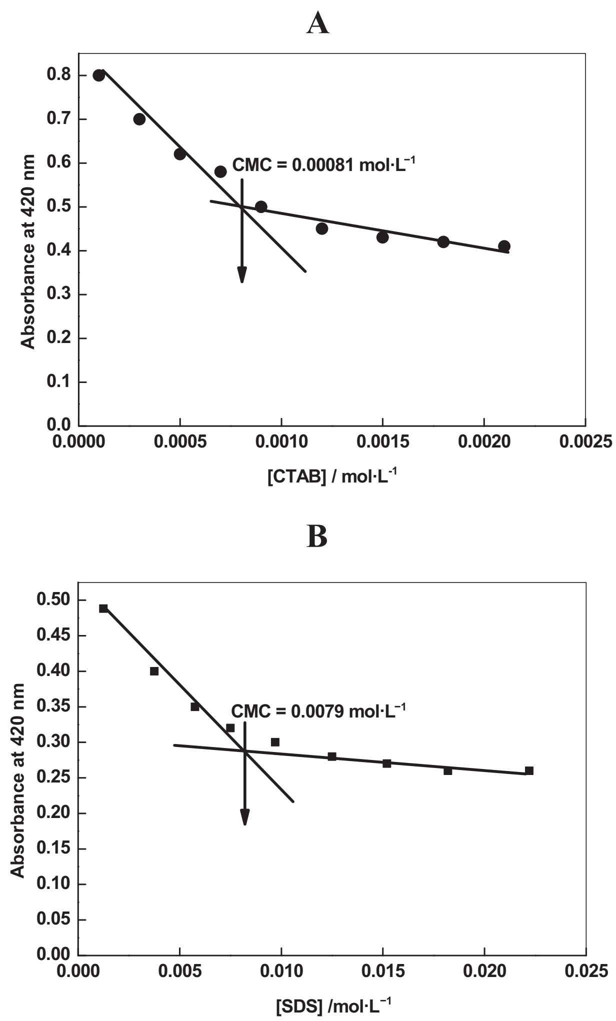

Fig. 9. Plot of absorbance as a function of [CTAB] (A) and [SDS] (B) for the solubilization of lawsone. Reaction conditions: [lawsone] = 4.0×10^{-4} mol·L^{-1}.

$$\Delta(\text{Absorbance}) = -\frac{[\text{surfactant}][\text{Lawsone}]}{\Delta(\text{Absorbance})} \times \alpha^2 + ([\text{surfactant}] + [\text{Lawsone}]) \times \alpha + \frac{\alpha}{K_S} \quad (5)$$

By substituting the values of Δ(Absorbance) and [surfactant] (=12.0×10^{-4} and 12.5×10^{-3} for CTAB and SDS) in Eq.(5), the K_S were also calculated for both surfactant and found to be 1.2×10^3 and 7.4×10^2 L·mol^{-1}, respectively. Inspection of Table 1 clearly suggested that the K_S values calculated by three different models are in same magnitude as CTAB and slightly different for SDS. The surfactant-lawsone complex formation constant was higher with CTAB than that of SDS, indicating that the lawsone molecules are solubilized in inner palisade layer of micelles (Fig. 5). The incorporation of lawsone molecules into the micelles is facilitated because anionic species of lawsone are attracted by the cationic head group of CTAB. On the other hand, such type of situation does not persist in presence of SDS. The repulsion forces between the same-charged dye and surfactant were stronger than other interactions exist in the dye-micellar system. Due to the electrostatic repulsion, lawsone molecules orientation is more likely in outer Stern layer of SDS micelles close to micelle water interface (Fig. 6).

Before going to calculate the concentration of incorporated lawsone into the micelles, it is essential to evaluate the critical micellar concentrations (CMC) of CTAB and SDS. Surfactant behaves as an electrolyte at lower concentration. They formed aggregates at a specific concentration, these aggregates called micelles, which has many layers (Stern layer, palisade layer, hydrophobic core and Gouy-Chapman layer) for the incorporation and/or solubilization of hydrophobic and hydrophilic compounds through different possible interactions. Absorbance of lawsone at 420 nm was found to decreases with increasing [surfactant]. These results are supplemented in Table ST1 (Supplementary Material). The changes of dye absorbance with increasing surfactant concentrations were used for the CMC determination [43]. The intersection of the two straight lines on the concentration plot gives CMC (Fig. 9A and B). Our CMC values are in accordance with the literature values [44–46].

The [lawsone] into the surfactant (L_m) was evaluated by using Eq. (6)).

$$[L_m] = \frac{(A_0 - A)}{(\varepsilon_0 - \varepsilon_m)} \quad (6)$$

where $\varepsilon_0 - \varepsilon_m = \Delta\varepsilon$. For the calculation of [m] (=micellar concentration) and n (=approximate number of lawsone incorporated into the micelle), the following relations were used (Eqs. (7) and (8)) [47].

$$n = \frac{[L_m]}{[m]} \quad (7)$$

$$[m] = \frac{[\text{surfactant}] - \text{CMC}}{N_{\text{aggregation}}} \quad (8)$$

where $N_{\text{aggregation}}$ = mean aggregation number of surfactant (=80 and 63 for CTAB and SDS [47,48]. Table 1 shows the 2.2×10^{-4} and 3.1×10^{-4} 4 mol·L^{-1} of lawsone are solubilized in [CTAB] = 1 2.0×10^{-4} 4 mol·L^{-1} and [SDS] = 12.5×10^{-3} 4 mol·L^{-1} micellar aqueous pseudo-phase at 30 °C. The [lawsone] = ca. 1.8×10^{-4} 4 mol·L^{-1} remains in the water. The number of incorporated lawsone is higher for cationic micelles (n = 44) than for anionic micelles (n = 4).

The pH of the micellar surface play an significant role in the the solubilization of ionic species into the stern layer and/or core. A series of experiments were performed to observe the change in the pH of the lawsone solution with CTAB and SDS. The pH values was found to be constant (pH = 6.7) with addition of both surfactant. Tondra *et al.* reported that the control of pH is not straightforword in micellar solutions [49,50]. The pH of the anionic and cationic micellar surface is ca. 2 units less and more than the aqueous bulk solvent, repectively. Thus, we assume that pH of the CTAB and SDS micellar surface should be ca. 9 and 5 under our experimental conditions [50,51]. The large number of lawsone molecules incorporated into the CTAB micelles through electroistatic interaction between the lone pairs electrons carbonyl oxygen as well as negative oxygen of lawsone and positive head group of CTAB micelles. On the other hand, electristic repulsion might be persist in presence of SDS. Lawsone is solubilized via hydrophobic interactions into the SDS. The change in the standard free energy (ΔG^0) are calculated by using Eq. (9).

$$\Delta G^0 = -RT\ln K_S \tag{9}$$

where R and T are the gas constant and temperature in Kelvin. The ΔG^0 are given in Table 1, indicating that the solubilization process is spontaneous. Figs. 5 and 6 clearly show that the lawsone solubilisations into the micelles are slow. The absorbance decreases with time and remains constant after ca. 50 min. The decay became slow at higher reaction time (Fig S2; supporting information). We did not observe the rate of solubilisation at higher [CTAB] ($\geq 25.0 \times 10^{-4}$ mol·L^{-1}). The solubilisation rate constants were calculated by using pseudo-first rate-law (Fig. 10), which indicates that rate of lawsone solubilisation decreases with [CTAB].

Lawsone has unique properties (complex formation [3], intramolecular hydrogen bonding [52] and redox activity [53]) due to the presence of two carbonyl groups at C1 and C4 with one OH group at C2. Its redox activities (one and two electron oxidation-reduction with and without proton transfer) depends on the experimental conditions [6,21,53]. In the present study, we reported the lawsone-surfactant complex formation between the opposite and same charged CTAB and SDS surfactants with spectroscopic measurements. Lawsone solubilized into the aggregates of CTAB and SDS through electroistatic, hydrophobic and van der Walls interactions. Thus we may stated confidently that the lawsone acted as a dye under our experimental conditions, which is the most important property of lawsone.

3.2. Tensiometry data

Surface active agents reduced the surface tension of water (γ_0 = 73 mN·m^{-1}) to some extent (γ) and formed various aggregates (monomer, dimer and trimmer, etc.). In the present study, all surface parameters were calculated such as CMC, surface tension at the CMC (π), surface pressure (π_{CMC}), surface excess (Γ_{max}) and minimum area per molecule (A_{min}) were calculated with Gibbs equation (Eqs. (10)–(12)) for pure surfactants and with dye.

$$\pi_{CMC} = \gamma_0 - \gamma_{CMC} \tag{10}$$

$$\Gamma_{max} = \left(-\frac{1}{2.303nRT}\right) \times \left(\frac{d\gamma}{d\ \lg[\text{surfactant}]}\right) \tag{11}$$

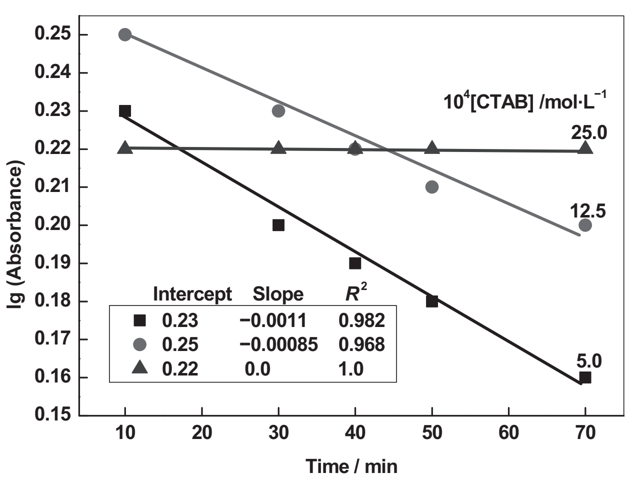

Fig. 10. First-order plots for the solubilization of lawsone into CTAB. Reaction conditions: [lawsone] = 4.0 × 10^{-4} mol·L^{-1}.

$$A_{min} = \frac{10^{20}}{N_A \Gamma_{max}} \tag{12}$$

The standard free energy change for the surfactant aggregation (ΔG^0_{ag}), bulk to the surface (ΔG^0_{ad}) and free energy at the junction of air–water (G_{min}) were estimated with the following equations. These values are given in Table 2.

$$\Delta G^0_{ag} = -RT\ln \text{CMC} \tag{13}$$

$$\Delta G^0_{ad} = \Delta G^0_{ag} - 6.023\pi_{CMC}A_{min} \tag{14}$$

$$G_{min} = A_{min} \times \gamma_{CMC} \times 6.022 \times 10^{23} \tag{15}$$

Upon addition of CTAB (from 1.0×10^{-4} to 25.0×10^{-4} mol·L^{-1} in a fixed [lawsone] (=4.0 × 10^{-4} mol·L^{-1}), surface tension sharply and slowly decreases at lower and higher CTAB concentrations, respectively (Fig. 11A). For SDS, surface tension was also decreases with [SDS] and became constant at higher concentration (Fig. 11B). CMC values were calculated from the Fig. 11A and B. The observed variations of surface tension above the CMC were negligible [36]. The optimal surfactant configuration in the micelle was more complicated [54,55]. It was observed that the CMC of CTAB decrease from 7.8×10^{-4} mol·L^{-1} to 6.0×10^{-4} mol·L^{-1} with the addition of lawsone, decreases in CMC might be due to the incorporation of dye into the micellar aggregates through ionic and hydrophobic interactions [56].

The various factors such as equilibrium between dye aggregates (monomer ↔ dimer), surfactant monomer, micelles, dye surfactant permicellar region and dye molecules incorporated into the micelles are operates simultaneously during the dye-surfactant interactions [39]. Micelles are not fixed entities and they have transient character. A decrease in CMC and reduction of surface tension on the addition of lawsone suggests the formation of dye-surfactant complex through the binding of surfactants to lawsone. The surface tension relaxation in CTAB-lawsone system might be due to the slow solubilization, which is dynamic in nature. Due to non-rigid structure of micelles and imbalance hydrophilic-hydrophobic forces, lawsone present in the different layers of micelles. The exact position of lawsone within CTAB micelles is not fixed owing to dynamic nature of solubilization process [57].

The π_{CMC}, Γ_{max} and A_{min} were calculated with Eqs. (13) and (14) for both CTAB and SDS, and indicating that the lawsone-CTAB system is moreat the binary boundary of the air–water interface. Higher value of A_{min} indicates the ion-pair and/or complex formation between the dye and micelles [58]. Table 2 shows that change in free energy (ΔG^0_{ag}) and (ΔG^0_{ad}) are negative might be due to spontaneous and endothermic solubilization. ΔG^0_{ad} and ΔG^0_{ag} ratio also suggested the formation of mono layer between CTAB and dye. On the other hand, the lower G_{min} signify the formation of stable air–water surface.

Surfactant behaves as an electrolyte at lower concentration. CTAB ionized in water and dynamic equilibrium exists between the ionized and unionized molecules (CTAB ⇌ CTA^+ − B^-). The degree of counter ion dissociation (β) of the micelle was calculated from the ratio of the slopes of the post-micellar (S_2) and premicellar (S_1) regions before and after the addition of lawsone in the CTAB solution near its CMC [57]. The values of β was found to be 0.25 and 0.40 for CTAB and CTAB + lawsone, respectively, indicating that the β is higher in presence of lawsone than in its absence. This may be due to the solubilization of lawsone in the palisade layer of cationic CTAB micelles. It has been established that the solubilizing capacity of micellar system can be enhanced using two or more different surfactants [59]. The mixed micellar system can be changes the morphology of micelle and improved their properties. Mixed micellar system of nonionic – nonionic and ionic-nonionic

Table 2
Values of surfactant-lawsone solubilization parameters calculated by surface tension data 30 °C

Parameters	CTAB	CTAB + lawsone	SDS	SDS + Lawsone
CMC/mol·L^{-1}	7.8×10^{-4}	6.0×10^{-4}	7.9×10^{-3}	7.2×10^{-3}
π/mN·m^{-1}	38.5	35.0	40.1	39.3
π_{CMC}/mN·m^{-1}	34.5	38.0	32.9	33.7
Γ_{max}/mol·m^{-2}	6.4×10^{-6}	6.7×10^{-6}	8.1×10^{-6}	7.9×10^{-6}
A_{min}/nm	2.52	2.64	4.14	4.11
G_{min}/kJ·mol^{-1}	57.4	53.6	11.5	10.2
ΔG^0_{ag}/kJ·mol^{-1}	−18.4	−18.6	−12.2	−12.4
ΔG^0_{ad}/kJ·mol^{-1}	−24.2	−24.6	−20.2	−20.3
K_{ag}	14.8×10^2	16.0×10^2	1.2×10^2	1.3×10^2
K_{ad}	14.8×10^3	17.3×10^3	3.0×10^3	3.1×10^3
$K_{ad\text{-}ag}$	9.9	11.0	23.9	23.0
$\Delta G^0_{ad}/\Delta G^0_{ag}$	1.3	1.3	1.6	1.6

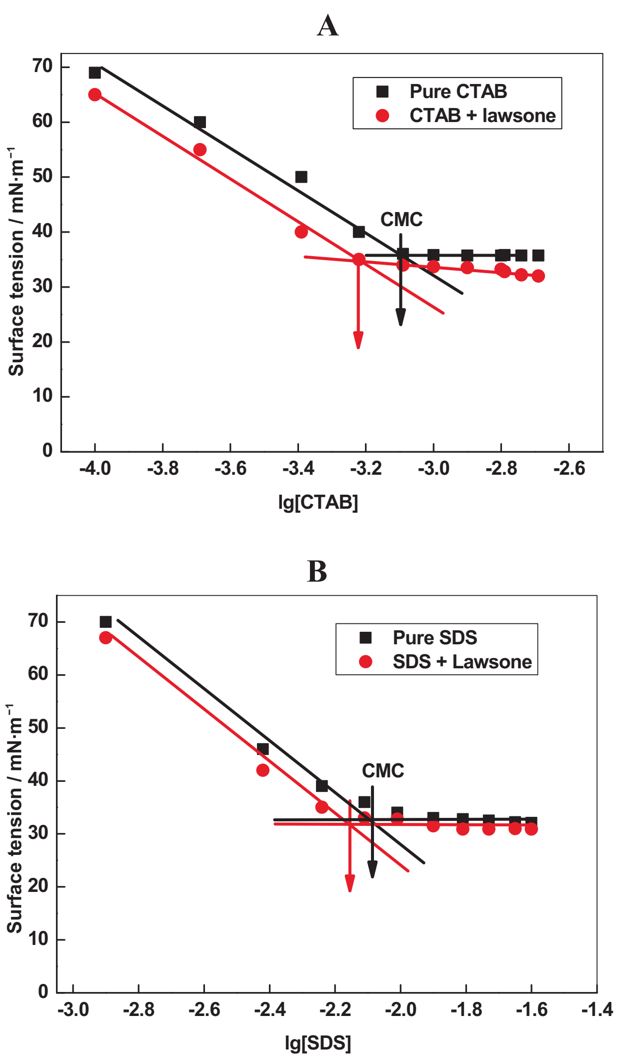

Fig. 11. Plots of surface tension *versus* lg[CTAB] (A) and lg[SDS] (B) with and without lawsone. Reaction conditions: [lawsone] = 4.0×10^{-4} mol·L^{-1}.

surfactants will get an edge over the mixture of ionic surfactants for the dye solubilization [60]. In the present study, CTAB-SDS mixed micellar system formed pseudo-nonionic micelles, which inhibits the incorporation of lawsone into the micelles due to the alternate arrangement of cationic and anionic aggregates at the micellar head group polar region. The detailed investigations on lawsone dye solubilization into the mixed micellar system (nonionic- nonionic, ionic-nonionic and ionic-ionic) are in progress for enhanced red color stability and color fastness.

3.3. Dye adsorption on glass surface

Metal ions have strong adsorption efficiency for the removal of dyes from an aqueous solution [26,28,61]. In order to determine the sensing and mordant ability of Ag^+, Cu^{2+}, Zn^{2+}, Ni^{2+}, Co^{2+}, Fe^{3+} and Al^{3+} towards lawsone, each metal ion was added in a reaction solution containing lawsone, CTAB and NaOH at 30 °C. No deposition of solid red was observed at the bottom of the reaction flask (Table 3). On the other hand, dye adsorption start at the bottom of the reaction flask upon addition of NaOH in a reaction mixture of lawsone, CTAB and silver ions. UV–visible spectra are recorded at different time intervals (Fig. 12), which clearly indicates that solid red material completely deposited on the glass surface and aqueous solution became perfect transparent with in ca. 90 min. Inspection of optical images clearly suggested that the reaction flask has two layers (deposited of solid on the glass surface and aqueous layer). Thus, lawsone displays an excellent selectivity for Ag^+ over other complex forming metal ions.

Lawsone formed complex with transition metal ions in presence of a mild base [3]. The deprotonation of C2-OH of lawsone is essential for the coordination with metal ions. Transition metal ions (Al^{3+}, Co^{2+}, Cu^{2+}, Fe^{3+}, Ni^{2+} and Zn^{2+}) formed hydroxide at higher pH, which diminished the possibility to the ionization of lawsone. The deposition of solid red materials was observed at higher pH only with Ag^+ ions (Table 3). The lawsone-Ag^+ complex was solubilized into the micelles of CTAB and deposited on the surface of glass via van der Walls forces simultaneously. Silver ions acted as a sensor and dye mordant for lawsone under our conditions. A preliminary study showed that adsorption of a red color layer of dye on to the surface of reaction flask is slow. Therefore,

Table 3
Adsorption of metal ions with lawsone (red color) on the surface of glass in presence of CTAB

Metal ion	pH	Observation
Na^+	6.7	No red dye deposition
K^+	6.7	No red dye deposition
Ag^+	5.1	No red dye deposition
Ag^+	6.7	No red dye deposition
Ag^+	9.1	Red dye deposition
Ag^+	11.2	Red dye deposition
Ag^+	12.2	Red dye deposition
Zn^{2+}	11.2	No red dye deposition
Cu^{2+}	11.2	No red dye deposition
Co^{2+}	11.2	No red dye deposition
Ni^{2+}	11.2	No red dye deposition
Fe^{3+}	11.2	No red dye deposition
Al^{3+}	11.2	No red dye deposition

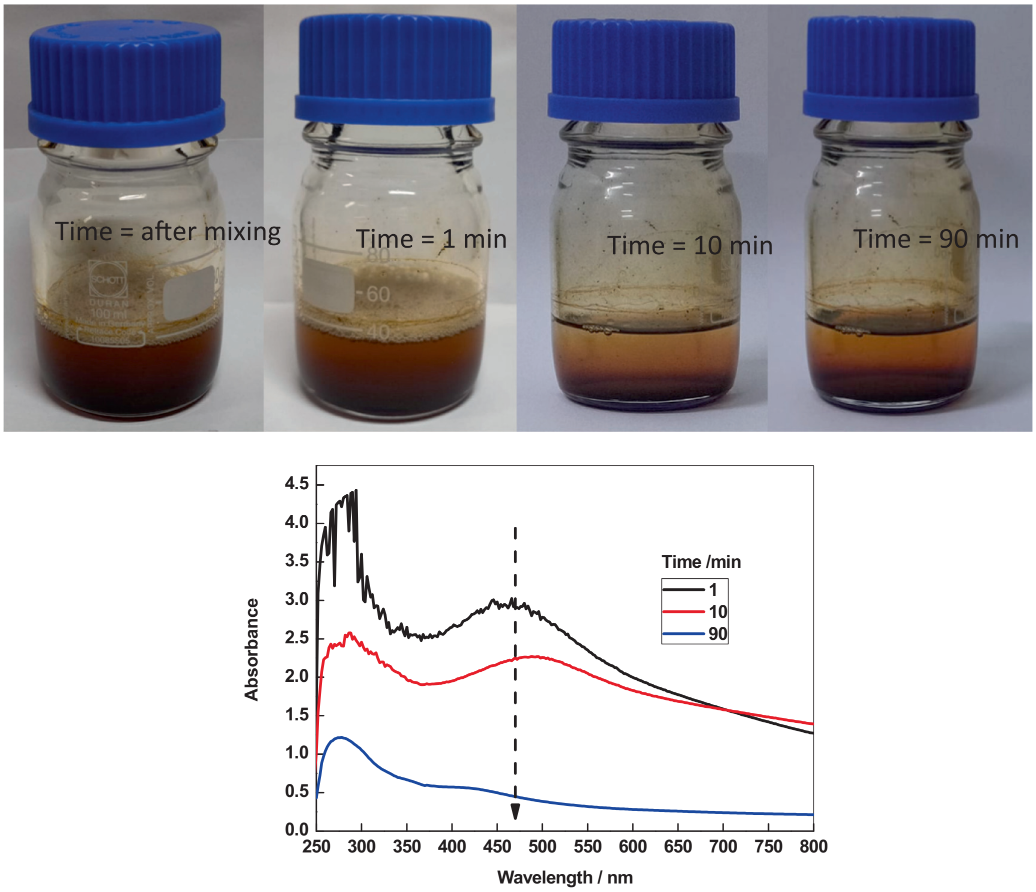

Fig. 12. Optical images and UV–visible spectra showing the deposition of lawsone dye onto the surface of glass as a function of time. Reaction conditions: [lawsone] = 4.0×10^{-4} mol·L^{-1}, [CTAB] = 12.5×10^{-4} mol·L^{-1}, [Ag^+] = 5.0×10^{-4} mol·L^{-1} and [NaOH] = 5.0×10^{-3} mol·L^{-1}.

the amount of adsorbed dye was estimated as a function of time with Eqs. (16 and 17).

$$q_t = \frac{([\text{lawsone}]_0 - [\text{lawsone}]_t)}{W}V \quad (16)$$

$$q_e = \frac{([\text{lawsone}]_0 - [\text{lawsone}]_e)}{W}V \quad (17)$$

where q_t and q_e are the amount of adsorbed dye at time t, and at the end of the adsorption, respectively. V = volume of the solution and W = mass of the adsorbent (silver nanoparticles). The various adsorption parameters (intra particle diffusion ($k_{\text{diffusion}}$), thickness of boundary layer (I), initial adsorption (α), pseudo-first order(k_1), pseudo-second-order (k_2) rate constants, and desorption constant (β) were estimated by using the following Eqs.

$$\ln(q_e - q_t) = \ln q_e - k_1 t \quad (18)$$

$$\frac{t}{q_t} = \frac{t}{q_e} + \frac{1}{k_2 q_e^2} \quad (19)$$

$$q_t = I + k_{\text{diffusion}} t^{\frac{1}{2}} \quad (20)$$

$$q_t = \frac{1}{\beta}\ln(t) + \frac{1}{\beta}\ln(\alpha\beta) \quad (21)$$

The k_1 and k_2 were calculated from Lagergren plot (Fig. 13A; ln (q_e–q_t) versus time) and pseudo-second-order plot (Fig. 13B; t/q_t *versus* time), respectively, and are given in Table 4 along with the corresponding R^2 (linear regression correlation coefficient). Lawsone adsorption followed the pseudo-second-order kinetics (Eq. (19)) with 0.993 R^2, which is higher than that of Lagergren model (R^2 = 0.992; Table 4) [62].

Intraparticle diffusion kinetic rate law (Weber and Morris model [63]) was also used to determine the nature of adsorption mechanism and thick ness of surface layer. According to the Eq. (20), the Weber-Morris plot (q_t *versus* $t^{1/2}$) should be linear with positive intercept. The values of $k_{\text{diffusion}}$ (0.965 mg·g^{-1}·min^{-1}) and I (11.08 mg·g^{-1}) were calculated from the slope and intercept of Fig. 13C. The presence of intercept indicated that the adsorption of lawsone on the surface of adsorbent is not a rate-determining step (characteristic of intraparticle diffusion mechanism). The positive value of I also suggested that film diffusion might be responsible for the adsorption of lawsone. The R^2 (=0.965) is also lower than R^2 (=0.993) of pseudo-second-order kinetic model. Thus, we may state that the adsorption of lawsone proceeds through the ionization, association, complexation, external mass transportation and others [64].

In order to confirm the multilayer adsorption of lawsone on the silver nanoparticles, the Elocivh kinetic model [65] was also applied for the calculation of associated parameters (α = initial adsorption rate constant and β = desorption constant), which was found to be 0.36 and 43.3, respectively with low R^2 (=0.946), which is lower than that of pseudo-first, second-order and intraparticle diffusion models. The Elovich plot (Fig. 13D; q_t *versus* ln (t)) was deviated from the linearity, which indicated that the lawsone adsorption occurred only via mono-layer formation and not obeys the multilayer adsorption. Optical image of the deposited red

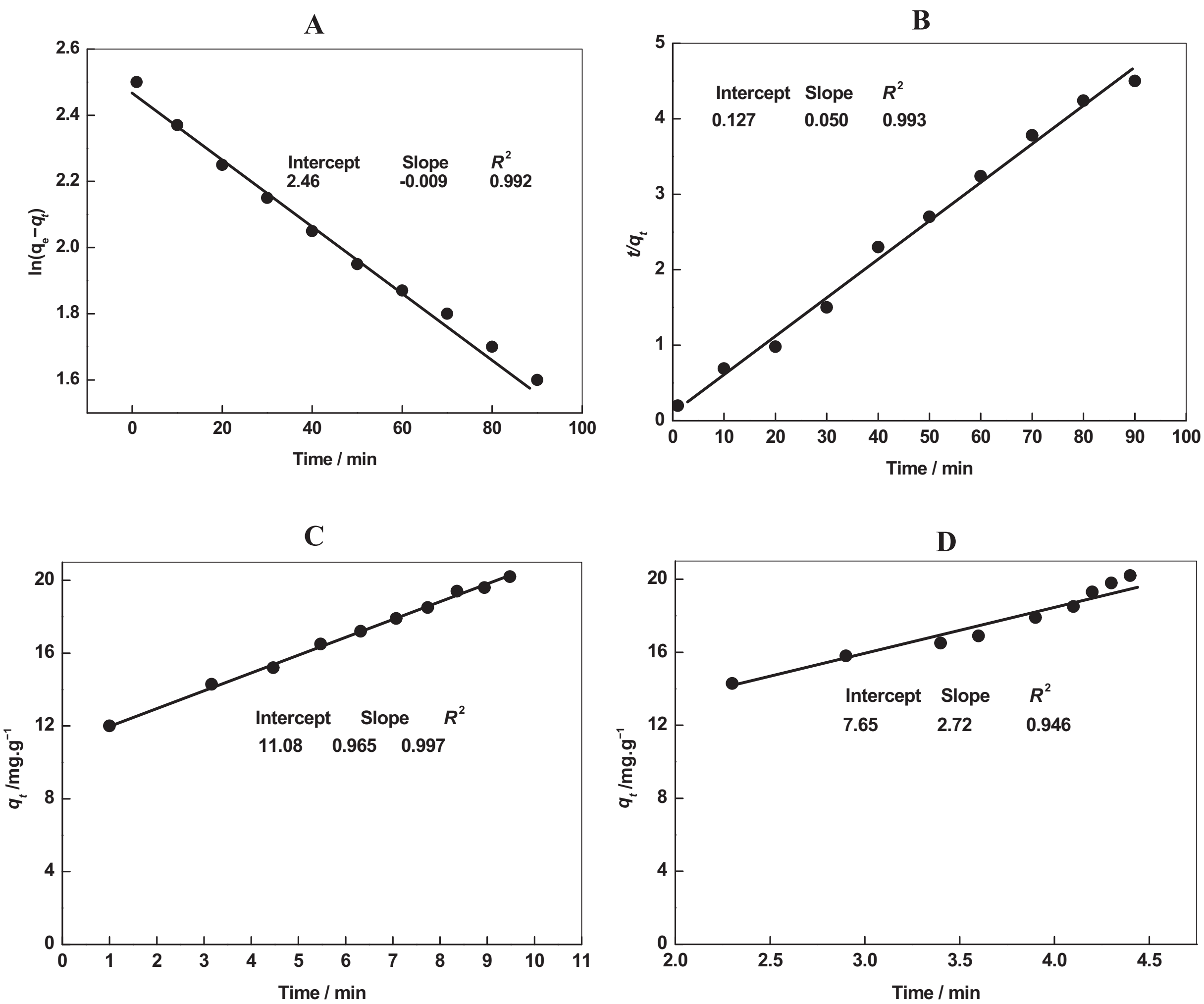

Fig. 13. Adsorption kinetic plots: (A) Pseudo-first-order, (B) pseudo-second-order, (C) intraparticle diffusion and (D) Elovich) for the deposition of lawsone on the glass surface.

Table 4
Values of lawsone adsorption kinetic parameters on the surface of silver nanoparticles 30 °C

Kinetic models	Parameters	Values
Pseudo-first-order equation:	Intercept	2.46
$\ln(q_{e,\,exp} - q_t) = \ln(q_e) - k_1 t$	Slope	−0.009
Plot $(q_e - q_t)$ *versus* time	q_e/mg·g^{-1}	11.7
Intercept = $\ln(q_e)$	k_1/min^{-1}	0.009
Slope = $-k_1$	R^2	0.992
Pseudo-second-order equation:	Intercept	0.127
$t/q_t = 1/k_2\, q_e^2 + t/q_e$	Slope	0.050
Plot t/q_t *versus* time	q_e/mg·g^{-1}	20.0
Intercept = $1/k_2 q_e^2$	k_2/g·mg^{-1}·min^{-1}	0.019
Slope = $1/q_e$	R^2	0.993
Interparticle diffusion equation:	Intercept	11.08
$q_t = k_{diffusion}\, t^{1/2} + I$	Slope	0.965
Plot q_t *versus* $t^{1/2}$	I/mg·g^{-1}	11.08
Intercept = I	$k_{diffusion}$/mg·g^{-1}·min^{-1}	0.965
Slope = $k_{diffusion}$	R^2	0.997
Elovich equation:	Intercept	7.65
$q_t = 1/\beta \ln(\alpha\beta) + 1/\beta \ln t$	Slope	2.72
q_t *versus* $\ln t$	β/mg·g^{-1}	0.36
Intercept = $1/\beta \ln(\alpha\beta)$	α/mg·g^{-1}·min^{-1}	43.3
Slope = $1/\beta$	R^2	0.946

lawsone on the surface of glass and schematic adsorption of silver ions, lawsone and CTAB is summarized in Fig. 14.

To the better presentation of lawsone adsorption, reverse optical image of reaction vessel is given in Fig. 15, which clearly demonstrates the complete adsorption of dye on to the surface of glass and aqueous water layer became perfect transparent.

4. Conclusions

In this study, the lawsone was extracted from the fresh Henna leaves, and added into the ionic surfactants and investigated for dye solubilisation into the sub- and post-micellar aggregates. The dye-surfactant solubilisation constants and number of lawsone molecules solubilized in micelles estimated and showed that the interactions between lawsone and CTAB are very strong than that of SDS. The number of solubilized dye molecules are also much higher in CTAB, which revealed that electrostatic interactions paly in significant role during the lawsone solubilisation than hydrophobic interactions. The intensity of color increases in an alkaline media. Silver ions acted as an excellent dye adsorbent and deposition of lawsone red color occurred with time on the surface of reaction vessel. Adsorption kinetic models (Lagergren, pseudo-second order, intraparticle diffusion and multilayer Elo-

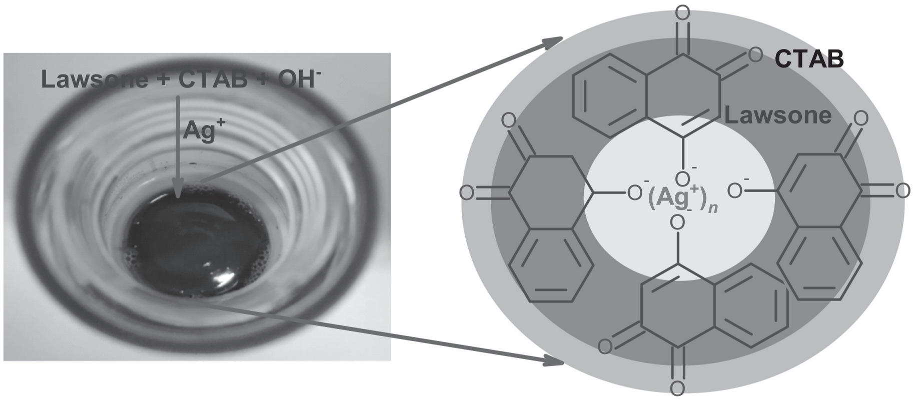

Fig. 14. Optical image and probable schematic adsorption of dye on the surface of glass.

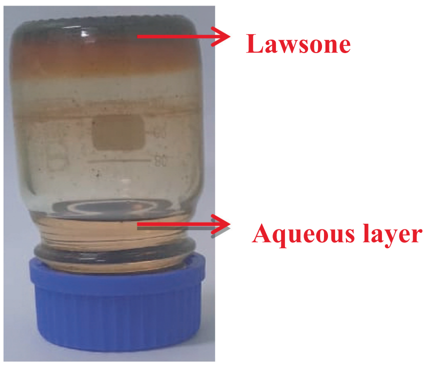

Fig. 15. Reverse optical image showing the adsorption of dye on glass surface.

vich) were applied. Lawsone adsorption kinetics followed pseudo-second order and intraparticles diffusion models. Our findings would be helpful to enhance the color fastness of textile dyeing process with a suitable surfactant and metal ion as a mordant.

Declaration of Competing Interest

The authors declare that they have no known competing financial interests or personal relationships that could have appeared to influence the work reported in this paper.

Acknowledgements

This work was supported by the Deanship of Scientific Research (DSR), King Abdulaziz University, Jeddah, grant No. (G: 255-247-1440). The authors, therefore, gratefully acknowledge the DSR technical and financial support.

Supplementary Material

Supplementary data to this article can be found online at https://doi.org/10.1016/j.cjche.2020.09.064.

References

[1] G. Chaudhary, S. Goyal, P. Poonia, Lawsonia inermis linnaeus: A phytopharmacological review, *Int. J. Pharm. Sci. Drug Res.* 2 (1) (2010) 91–98.
[2] M. Dabiri, Z.N. Tisseh, A. Bazgir, Synthesis of fluorescent hydroxyl naphthalene-1,4-dione derivatives by a three-component reaction in water, *Dyes Pigm.* 89 (1) (2011) 63–69.
[3] S. Salunke-Gawali, E. Pereira, U.A. Dar, S. Bhand, Metal complexes of hydroxynaphthoquinones: Lawsone, bis-lawsone, lapachol, plumbagin and juglone, *J. Mol. Struct.* 1148 (2017) 435–458.
[4] G. Valle-Bourrouet, V.M. Ugalde-Saldivar, M. Gomez, L.A. Ortiz-Frade, I. Gonzalez, C. Frontana, Magnetic interactions as a stabilizing factor of semiquinone species of lawsone by metal complexation, *Electrochim. Acta* 55 (28) (2010) 9042–9050.
[5] F.L.S. Bustamante, M.M.P. Silva, W.A. Alves, C.B. Pinheiro, J.A.L.C. Resende, M. Lanznaster, Isomerism and nuclearity control in bis(lawsonato)zinc(II) complexes, *Polyhedron* 42 (1) (2012) 43–49.
[6] Y.M. Hijji, B. Barare, Y. Zhang, Lawsone (2-hydroxy-1,4-naphthoquinone) as a sensitive cyanide and acetate sensor, *Sens. Actuators B Chem.* 169 (1) (2012) 106–112.
[7] M. Sonawane, K. Tayade, S.K. Sahoo, C.P. Sawant, A. Kuwar, A new lawsone azo-dye for optical sensing of Fe^{3+} and Cu^{2+} and their DFT study, *J. Coord. Chem.* 69 (18) (2016) 2785–2792.
[8] R. Jelly, S.W. Lewis, C. Lennard, K.F. Lim, J. Almog, Lawsone: A novel reagent for the detection of latent fingermarks on paper surfaces, *Chem. Comm.* (30) (2008) 3513–3515.
[9] J. Almog, Y. Cohen, M. Azoury, T.-R. Hahn, Genipin-A novel fingerprint reagent with colorimetric and fluorogenic activity, *J. Forensic Sci.* 49 (6) (2004) 1–3.
[10] Y. Nemoto, H. Funahashi, The interaction between acid dye and nonionic surfactant, *J. Colloid. Interf. Sci.* 62 (1) (1977) 95–100.
[11] E. Barni, P. Savarino, G. Viscardi, Dye-surfactant interactions and their applications, *Acc. Chem. Res.* 24 (4) (1991) 98–103.
[12] B. Simoncie, M. Kert, A study of anionic dye- cationic surfactant interactions in mixtures of cationic and non-ionic surfactants, *Dyes Pigm.* 54 (3) (2002) 221–224.
[13] B. Simoncic, M. Kert, Influence of the chemical structure of dyes and surfactants on their interactions in binary and ternary mixture, *Dyes Pigm.* 76 (1) (2008) 104–112.
[14] S. Chandravanshi, S.K. Upadhyay, Natural dye -surfactant interaction; ther-modynamic and surface parameters, *Colora. Technol.* 128 (4) (2012) 300–305.
[15] S. Baliarsingh, A.K. Panda, J. Jena, T. Das, N.B. Das, Exploring sustainable technique on natural dye extraction from native plants for textile: identification of colourants, colourimetric analysis of dyed yarns and their antimicrobial evaluation, *J. Clean. Prod.* 37 (2012) 257–264.
[16] S. Baliarsingh, J. Jena, T. Das, N.B. Das, Role of cationic and anionic surfactants in textile dyeing with natural dyes extracted from waste plant materials and their potential antimicrobial properties, *Ind. Crops Prod.* 50 (2013) 618–624.
[17] R. Sharma, A. Kamal, R.K. Mahajan, Detailed study of interactions between eosin yellow and gemini pyridinium surfactants, *RSC Adv.* 6 (2016) 71692–71704.
[18] M. Yusuf, M. Shahid, M.I. Khan, S.A. Khan, M.A. Khan, F. Mohammad, Dyeing studies with henna and madder: a research on effect of tin (II) chloride mordant, *J. Saudi Chem. Soc.* 19 (1) (2015) 64–72.
[19] Z. Aksu, S. Ertugrul, G. Donmez, Methylene blue biosorption by rhizopus arrhizus: effect of SDS (sodium dodecylsulfate) surfactant on biosorption properties, *Chem. Eng. J.* 158 (3) (2010) 474–481.
[20] J. Sangeetha, J. Philip, Synthesis, characterization and antimicrobial property of Fe_3O_4-Cys-HNQ nanocomplex, with L-cysteine molecule as a linker, *RSC Adv.* 3 (21) (2013) 8047–8057.
[21] S.S. Khadtare, A.P. Ware, S. Salunke-Gawali, S.R. Jadkar, S.S. Pingale, H.M. Pathan, Dye sensitized solar cell with lawsone dye using ZnO photoanode: experimental and TD-DFT study, *RSC Adv.* 5 (2015) 17647–17652.
[22] S. Sreeja, B. Pesala, Plasmonic enhancement of betanin-lawsone co-sensitized solar cells via tailored bimodal size distribution of silver nanoparticles, *Sci. Rep.* 10 (2020) 8240.
[23] X. Li, W.C.H. Choy, H. Lu, W.E.I. Sha, A.H.P. Ho, Efficiency enhancement of organic solar cells by using shape-dependent broadband plasmonic absorption in metallic nanoparticles, *Adv. Funct. Mater.* 23 (21) (2013) 2728–2735.
[24] M. Barani, M. Mirzaei, M. Torkzadeh-Mahani, M.H. Nematollahi, Lawsone-loaded niosome and its antitumor activity in MCF-7 breast cancer cell line: A nano-herbal treatment for cancer, *DARU J. Pharm. Sci.* 26 (1) (2018) 11–17.

[25] G.S. Gupta, G. Prasad, V.N. Singh, Removal of chrome dye from aqueous solutions by mixed adsorbents: Fly ash and coal, *Water Res.* 24 (1) (1990) 45–50.
[26] S.-H. Kim, P.-P. Choi, Enhanced congo red dye removal from aqueous solutions using iron nanoparticles: Adsorption, kinetics, and equilibrium studies, *Dalton Trans.* 46 (44) (2017) 15470–15479.
[27] K.Y. Foo, B.H. Hameed, Insights into the modeling of adsorption isotherm systems, *Chem. Eng. J.* 156 (1) (2010) 2–10.
[28] A. Tor, Y. Cengeloglu, Removal of congo red from aqueous solution by adsorption onto acid activated red mud, *J. Hazard. Mater. B* 138 (2) (2006) 409–415.
[29] V.K. Gupta, A. Mittal, V. Gajbe, J, Mittal, Removal and recovery of the hazardous azo dye acid orange 7 through adsorption over waste materials: Bottom ash and de-oiled soya, *Ind. Eng. Chem. Res.* 45 (4) (2006) 1446–1453.
[30] M. Ozacar, I.A. Sengil, A kinetic study of metal complex dye sorption onto pine sawdust, *Process Biochem.* 40 (2) (2005) 565–572.
[31] M. Ghaedi, M.N. Biyareh, S.N. Kokhdan, S. Shamsaldini, R. Sahraei, A. Daneshfar, S. Shahriyar, Comparison of the efficiency of palladium and silver nanoparticles loaded on activated carbon and zinc oxide nanorods loaded on activated carbon as new adsorbents for removal of congo red from aqueous solution: Kinetic andisotherm study, *Mater. Sci. Eng.C* 32 (4) (2012) 725–734.
[32] Z. Zaheer, Eco-friendly walnut shell powder based facile fabrication of biogenic Ag-nanodisks, and their interaction with bovine serum albumin, *J. Photochem. Photobiolo. B: Biol.* 193 (2019) 8–17.
[33] S.A. Kosa, Z. Zaheer, Betanin assisted synthesis of betanin@silver nanoparticles and their enhanced adsorption and biological activities, *Food Chem.* 298 (2019) (12 pages) 125014.
[34] Z. Zaheer, A. Al-Asfar, E.S. Aazam, Adsorption of methyl red on biogenic Ag@Fe nanocomposities adsorbent : Isotherms, kinetics and mechanistic approach, *J. Mol. Liq.* 283 (2019) 287–298.
[35] A. Al-Asfar, Z. Zaheer, E.S. Aazam, Eco-friendly green synthesis of Ag@Fe bimetallic nanoparticles: Antioxidant, antimicrobial and photocatalytic degradation of bromothymol blue, *J. Photochem. Photobiolo., B: Biol.* 185 (2018) 143–152.
[36] U.S. Siddiqui, J. Aslam, W.H. Ansari, Kabir-ud-Din, Micellization and aggregation behavior of a series of cationic gemini surfactants (m-s-m type) on their interaction with a biodegradable sugar-based surfactant (octyl-_-D-glucopyranoside), *Colloids Surf. A: Physicochem. Eng. Asp.* 421 (2013) 164–172.
[37] R.B. Patwardhan, P.K. Dhakephalkar, B.A. Chopade, D.D. Dhavale, R.R. Bhonde, Purification and characterization of an active principle, lawsone, responsible for the plasmid curing activity of *Plumbago zeylanica* root extracts, *Front. Microbiol.* 9 (2018) 2618.
[38] M.A.R. Bhuiyan, A. Islam, A. Ali, M.N. Islam, Color and chemical constitution of natural dye henna (Lawsonia inermis L) and its application in the coloration of textiles, *J. Clean. Prod.* 167 (2017) 14–22.
[39] M. Bielska, A. Sobczynska, K. Prochaska, Dye–surfactant interaction in aqueous solutions, *Dyes Pigm.* 80 (2) (2009) 201–205.
[40] H.A. Benesi, J.H. Hildebrand, A spectrophotometric investigation of the interaction of iodine with aqromatic hydrocarbons, *J. Am. Chem. Soc.* 71 (8) (1949) 2703–2707.
[41] P.H. Connett, K.E. Wetterhahn, In vitro reaction of the carcinogen chromatewith cellular thiols and carboxylic acids, *J. Am. Chem. Soc.* 107 (914) (1985) 4282–4288.
[42] K.K. Karukstis, D.A. Savi, C.T. Loftus, N.D. D'Angelo, Spectroscopic studies of the interaction of methyl orange with cationic alkyltrimethylammonium bromide surfactants, *J. Colloid Interface Sci.* 203 (1998) 157–163.
[43] M.C. Carey, D.M. Small, Micellar properties of dihydroxy and trihydroxy bile salts: Effects of counterion and temperature, *J. Coll. Inter. Sci.* 31 (3) (1969) 382–396.
[44] C.A. Bunton, G. Savelli, Organic reactivity in aqueous micelles and similar assemblies, *Adv. Phys. Org. Chem.* 22 (1986) 213–309.
[45] S. Tascioglu, Micellar solutions as reaction media, *Tetrahedron* 52 (34) (1996) 11113–11152.
[46] C.A. Bunton, Reactivity in aqueous association colloids. Descriptive utility of the pseudophase model, *J. Mol. Liq.* 72 (1–3) (1997) 231–249.
[47] A.M. Awan, S.S. Shah, Hydrophobic interaction of amphiphilic hemicyanine dye with cationic surfactant and anionic surfactant micelles, *Colloids Surf. A: Physicochem. Eng. Asp.* 122 (1997) 97–101.
[48] H.M.P. De Oliveiro, M.H. Gehten, Characterization of mixed micelles of sodium dodecylsulfate and tetraoxyethylene dodecyl ether in aqueous solutions, *Langmuir* 18 (10) (2002) 3792–3796.
[49] R. Cierpiszewski, M. Hebrant, J. Szymanowski, C. Tondre, Copper(II) complexation kinetics with hydroxyoximes in CTAB micelles. Effect of extractant hydrophobicity and additives, *J. Chem. Soc., Faraday Trans.* 92 (1996) 249–255.
[50] C. Tondre, M. Hebrant, Micellar and microemulsion systems to perform heterogeneous reactions, biphasic extraction and solute transport, *J. Mol. Liq.* 72 (1–3) (1997) 279–294.
[51] C. Tondre, M. Boumezioud, Microemulsions as model systems to study the kinetics and mechanism of reactions occurring in the extraction of metal ions by lipophilic extractants: complexation of nickel(II) by 8-hydroxyquinoline and Kelex 100, *J. Phys. Chem.* 93 (2) (1989) 846–854.
[52] B. Amro, K. James, T. Turner, A quantitative study of dyeing with lawsone, *J. Soc. Cosmet. Chem.* 45 (1993) 159–165.
[53] N. Gurjar, K. Daniel, S. Sharma, V. Daniel, Acid base indicator property of lawsonia inerimes leaves, *J. Biomed. Pharm. Res.* 3 (3) (2014) 64–66.
[54] S.F. Burlatsky, V.V. Atrazhev, D.V. Dmitriev, V.I. Sultanov, E.N. Timokhina, E.A. Ugolkova, S. Tulyani, A. Vincitore, Surface tension model for surfactant solutions at the critical micelle concentration, *J. Colloid Interf. Sci.* 393 (2013) 151–160.
[55] M. Akram, S. Anwar, F. Ansari, I.A. Bhat Kabir-ud-Din, Bio-physicochemical analysis of ethylene oxide-linked diester-functionalized green cationic gemini surfactants, *RSC Adv.* 6 (2016) 21697–21705.
[56] Z. Khan, M.A. Malik, S.A. Al-Thabaiti, O. Bashir, T.A. Khan, Natural dye bolaform sugar-based surfactant: Self aggregation and mixed micellization with ionic surfactants, *Dyes Pigm.* 131 (2016) 168–176.
[57] M.J. Rosen, J.T. Kunjappu, Surfactants and Interfacial Phenomena, fourth ed., John Wiley & Sons, New Jersey, USA, 2012.
[58] M.S. Bakshi, G. Kaur, Mixed micelles of series of monomeric and dimeric cationic, zwitterionic, and unequal twin-tail cationic surfactants with sugar surfactants: a fluorescence study, *J. Colloid Interf. Sci.* 289 (2) (2005) 551–559.
[59] S. Ghosh, S. Mondal, S. Das, R. Biswas, Spectroscopic investigation of interaction between crystal violet and various surfactants (cationic, anionic, nonionic and gemini) in aqueous media, *Fluid Phase Equilibr.* 332 (2012) 1–6.
[60] S.K. Mehta, K.K. Bhasin, A. Kumar, S. Dham, Micellar behavior of dodecyldimethylethyl ammonium bromide and dodecyltrimethylammonium chloride in aqueous media in the presence of diclofenac sodium, *Coll. Surf. A: Physicochem. Eng. Asp.* 278 (2006) 17–25.
[61] S.A. Al-Thabaiti, E.S. Aazam, O. Bashir, Z. Khan, Aggregation of congo red with surfactants and Ag nanoparticles in an aqueous solution, *Spectrochim. Acta Part A: Mol. Biomol. Spectrosc.* 156 (2016) 28–35.
[62] V.K. Gupta, B. Gupta, A. Rastogic, S. Agarwald, A. Nayaka, Comparative investigation on adsorption performances of mesoporous activated carbon prepared from waste rubber tire and activated carbon for a hazardous azo dye-Acid Blue 113, *J. Hazard. Mater.* 186 (1) (2011) 891–901.
[63] W.J. Weber, J.C. Morris, Kinetics of adsorption on carbon from solution, *J. Sanit. Eng. Div. Am. Soc. Civ. Eng.* 89 (2) (1963) 31–59.
[64] M. Ghaedi, S. Hajjati, Z. Mahmudi, I. Tyagi, S. Agarwal, A. Maity, V.K. Gupta, Modeling of competitive ultrasonic assisted removal of the dyes - methylene blue and safranin-O using Fe_3O_4 nanoparticles, *Chem. Eng. J.* 268 (2015) 28–37.
[65] S.Y. Elovich, O.G. Larinov, Theory of adsorption from solutions of non electrolytes on solid (I) equation adsorption from solutions and the analysis of its simplest form, (II) verification of the equation of adsorption isotherm from solutions, *Izv. Akad. Nauk SSSR, Otd. Khim. Nauk.* 2 (1962) 209–216.